



# Encapsulation of camphor in cyclodextrin inclusion complex nanofibers via polymer-free electrospinning: enhanced water solubility, high temperature stability, and slow release of camphor

Asli Celebioglu<sup>1</sup>, Zeynep Aytac<sup>1</sup>, Mehmet Emin Kilic<sup>1</sup>, Engin Durgun<sup>1</sup>, and Tamer Uyar<sup>1,\*</sup> 

<sup>1</sup> Institute of Materials Science and Nanotechnology, UNAM-National Nanotechnology Research Center, Bilkent University, 06800 Ankara, Turkey

**Received:** 29 October 2017

**Accepted:** 9 December 2017

**Published online:**

18 December 2017

© Springer Science+Business Media, LLC, part of Springer Nature 2017

## ABSTRACT

Electrospinning of polymer-free nanofibers (NF) was successfully performed from inclusion complexes (ICs) of modified cyclodextrins [hydroxypropyl- $\beta$ -cyclodextrin (HP $\beta$ CD) and hydroxypropyl- $\gamma$ -cyclodextrin (HP $\gamma$ CD)] and camphor (HP $\beta$ CD/camphor-IC-NF and HP $\gamma$ CD/camphor-IC-NF). Although camphor is a volatile and hydrophobic essential oil component, the improvement in the aqueous solubility and thermal stability of camphor by inclusion complexation with cyclodextrins was confirmed by phase solubility diagram and thermal analysis, respectively. Moreover, fast-dissolving characteristics of electrospun CD/camphor-IC-NF webs were also observed. Computational modeling study shows preferential orientation of camphor is variable depending on the CD types. In addition, the interaction of camphor molecule is slightly stronger with HP $\gamma$ CD when compared to HP $\beta$ CD owing to the better allocation of guest (camphor) in host (CD) cavity originating from the better size match. Even though camphor has high volatility, significant amount of camphor was preserved in HP $\beta$ CD/camphor-IC-NF and HP $\gamma$ CD/camphor-IC-NF after electrospinning. The molar ratio of HP $\beta$ CD:camphor and HP $\gamma$ CD:camphor was determined as  $\sim 1.00:0.65$  and  $\sim 1.00:0.90$  in HP $\beta$ CD/camphor-IC-NF and HP $\gamma$ CD/camphor-IC-NF, respectively. In short, encapsulation of camphor in cyclodextrin inclusion complex nanofibers via polymer-free electrospinning was attained, and enhanced water solubility, high temperature stability, and slow release of camphor were achieved for CD/camphor-IC-NF.

Address correspondence to E-mail: tamer@unam.bilkent.edu.tr

## Introduction

Essential oils are widely used in medical, food, and cosmetic industry due to their unique characteristics such as being as antibacterial, antioxidant, antifungal, antiseptic, and fragrance compounds [1]. Since essential oils are mixtures of hydrophobic volatile aroma compounds, their processing is often problematic due to their highly volatile nature and their low water solubility. Thus, various encapsulation strategies are often applied to increase the efficiency and long-term shelf life of essential oils [2]. Having the advantage of being a room temperature process, electrospinning is becoming one of the promising encapsulation method, wherein variety of bioactive agents such as drugs, plant extracts, essential oils, flavors/fragrances, and food additives are encapsulated in the electrospun nanofiber matrix for possible applications in pharmaceuticals and foods [3, 4]. Electrospinning is a very practical technique in order to obtain nanofibers and nanofibrous materials from wide range of materials including polymers, blends, composites, etc. [3, 5]. Nanofibers/nanowebs produced via electrospinning possess unique properties including high surface-to-volume ratio and

nanoporous structure along with design flexibility and functionalization with additives [3, 5].

Cyclodextrins (CDs) (Fig. 1a, b) are cyclic oligosaccharides, which are well known by their non-covalent inclusion complexes with various compounds [6]. The native types of CDs are named as  $\alpha$ -CD,  $\beta$ -CD, and  $\gamma$ -CD having 6, 7, and 8  $\alpha$ -D-glucopyranoside units in their cyclic structure, respectively. Chemically modified CDs (i.e., hydroxypropyl-, methyl-, carboxymethyl-CDs) are of importance in terms of their high water solubility when compared to native CDs [7, 8]. CDs are used as molecular encapsulation agents since they can form inclusion complexes with variety of hydrophobic compounds (drugs, essential oils, organic compounds, food and cosmetic additives, etc.) [6–8]. The cyclodextrin inclusion complexation facilitates the high thermal stability for volatile compounds and enhances the water solubility of the hydrophobic guest molecules [6–8].

In general, electrospinning involves polymeric solutions in which active agents like food additives, drugs, etc., can be incorporated into polymeric nanofibrous matrix [3, 4]. Nevertheless, we have shown that electrospun polymeric nanofibrous

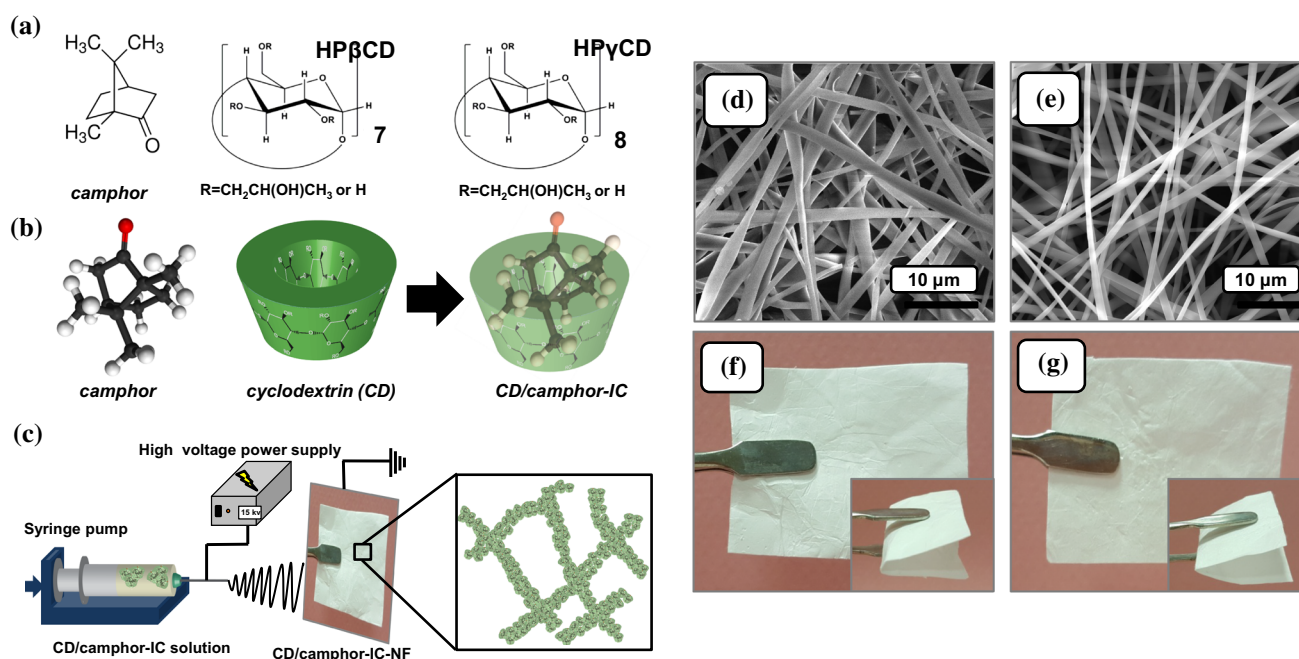


**Figure 1** a Chemical structure of camphor, HP $\beta$ CD, and HP $\gamma$ CD b schematic representation CD/camphor-IC formation and c electrospinning of CD/camphor-IC solution to produce CD/camphor-IC nanofibers (CD/camphor-IC-NF), representative SEM images

of electrospun nanofibers of d HP $\beta$ CD/camphor-IC-NF and e HP $\gamma$ CD/camphor-IC-NF; the photographs of nanofibrous webs of f HP $\beta$ CD/camphor-IC-NF and g HP $\gamma$ CD/camphor-IC-NF.

matrices are sometimes not very effective to preserve the volatile additives [9–12]. Therefore, in our recent studies, cyclodextrin inclusion complexes (CD-ICs) of many volatile/hydrophobic compounds were incorporated into electrospun polymeric nanofibers previously to overcome the volatility and stability problems associated with these active agents [9–12]. As an alternative approach to CD-IC-incorporated electrospun polymeric nanofibers, electrospinning of polymer-free nanofibers from CD-IC systems was also achieved by our group [13–20]. We have observed that the high aqueous solubility of modified CDs enables to obtain nanofibers from highly concentrated CD solutions [21, 22]. Therefore, CD-IC [13–20] solutions ultimately result in the formation of nanofibers due to the self-assembly and aggregation of CDs in their highly concentrated solutions.

Camphor (1,7,7-trimethyl-bicyclo[2.2.1]hepta-2-one) (Fig. 1a) is a white crystalline and natural compound, which is widely used in numerous industrial and pharmaceutical applications as a fragrance, food additive, and antidepressant, anti-inflammatory [23]. Camphor has a very low water solubility; moreover, camphor has a limited stability because it is a highly volatile compound having a rapid sublimation nature. Hence, the encapsulation of camphor is of great significance for its applications by preservation of its therapeutic efficacy. In this study, we achieved the encapsulation of camphor in cyclodextrin inclusion complex nanofibers via polymer-free electrospinning. That is, inclusion complexes of camphor with two different types of modified CDs [hydroxypropyl- $\beta$ -cyclodextrin (HP $\beta$ CD) and hydroxypropyl- $\gamma$ -cyclodextrin (HP $\gamma$ CD)] were electrospun into nanofibers (HP $\beta$ CD/camphor-IC-NF and HP $\gamma$ CD/camphor-IC-NF) as free-standing nanofibrous webs without using any polymeric fiber matrix (Fig. 1c). Enhanced water solubility, high temperature stability, and slow release of camphor were successfully achieved for these CD/camphor-IC-NF nanofibrous webs.

## Materials and methods

### Materials

Camphor ( $\geq 95\%$ , Sigma-Aldrich, Germany), deuterated dimethylsulfoxide (DMSO-d<sub>6</sub>, deuteration degree min 99.8% for NMR spectroscopy, Merck,

Germany), potassium bromide (KBr, 99%, FTIR grade, Sigma-Aldrich), hydroxypropyl-beta-cyclodextrin (HP $\beta$ CD, degree of substitution:  $\sim 0.6$ , Cavalol<sup>®</sup>W7 HP Pharma, kindly donated by Wacker Chemie (Germany)), and hydroxypropyl-gamma-cyclodextrin (HP $\gamma$ CD, degree of substitution:  $\sim 0.6$ , Cavalol<sup>®</sup>W8 HP Pharma, kindly donated by Wacker Chemie) were used as-received. The water was distilled/deionized from a Millipore Milli-Q ultrapure water system.

### Preparation of solutions for electrospinning

CD/camphor-IC solutions were prepared in aqueous solution (0.5 mL) by using two types of modified CD (HP $\beta$ CD and HP $\gamma$ CD) (0.8 g) and camphor (0.083 and 0.075 g) at 1:1 molar ratio. First, camphor powder was dispersed in water, then CDs [160% (w/v)] was added to the dispersions, and the resulting solutions were stirred at room temperature (RT) for 12 h. CD/camphor-IC solutions were turbid in the beginning; however, clear and homogenous solutions were achieved later on after the dissolution of camphor in the presence of CD in the aqueous solution. Finally, electrospinning was performed in order to produce nanofibers of HP $\beta$ CD/camphor-IC-NF and HP $\gamma$ CD/camphor-IC-NF in the form of self-standing nanofibrous webs. The composition, viscosity, and conductivity of CD/camphor-IC solutions and morphological characteristics of CD/camphor-IC nanofibers (CD/camphor-IC-NF) along with average fiber diameter (AFD) are summarized in Table 1. Pristine CD nanofibers without camphor (HP $\beta$ CD-NF and HP $\gamma$ CD-NF) were also produced as control samples according to our previous reports by electrospinning of aqueous HP $\beta$ CD and HP $\gamma$ CD solutions having 160% (w/v) concentration [21, 22].

### Electrospinning of nanofibers

CD/camphor-IC solutions in 1 mL plastic syringe (metallic needle having 0.4 mm inner diameter) were mounted on a syringe pump (KD Scientific, KDS-101, USA) and pumped at 0.5 mL/h rate toward a grounded metal collector covered with aluminum foil. The distance between the needle and the collector was 10–15 cm, and electric field (15–20 kV) was applied by using a high voltage power supply (AU Series, Matsusada Precision Inc., Japan). The electrospinning was performed in a horizontal setup in a

**Table 1** Properties of the CD/camphor-IC solutions used for electrospinning and morphological characteristics of the resulting CD/camphor-IC nanofibers

Solutions	% CD <sup>a</sup> (w/v)	% camphor <sup>b</sup> (w/w)	Viscosity (Pa·s)	Conductivity (μS/cm)	Average fiber diameter (nm)	Fiber morphology
HPβCD/camphor-IC	160	9.4	0.52	15.29	1330 ± 440	Bead-free nanofibers
HPγCD/camphor-IC	160	8.4	0.37	7.95	1110 ± 305	Bead-free nanofibers

<sup>a</sup>With respect to solvent (water)

<sup>b</sup>With respect to total weight of the sample

Plexiglas box at 25 °C and 18% relative humidity. After electrospinning, the electrospun CD/camphor-IC-NF (HPβCD/camphor-IC-NF and HPγCD/camphor-IC-NF) webs and pure CD-NF (HPβCD-NF and HPγCD-NF) webs were kept in refrigerator (+ 4 °C) prior to their analyses.

### Measurements and characterization

Phase solubility test was performed according to the method of Higuchi and Connors [24]. An excess amount of camphor was added to aqueous CD (HPβCD and HPγCD) solutions, and the suspensions were shaken at RT. After equilibrium was achieved at the end of 48 h, the suspensions were filtered with 0.45 μm membrane filter. The absorption of the solutions was determined at 286 nm by UV spectroscopy (Varian, Cary 100). The absorption values were converted into the concentration of camphor by the solubility of camphor without CDs [25]. The experiments were carried out in triplicate, and the results were reported as average ± standard deviation.

The stability constant ( $K_C$ ) was calculated based on the phase solubility diagram according to the following equation:

$$K_C = \text{slope}/S_0(1 - \text{slope}), \quad (1)$$

where  $S_0$  is the intrinsic solubility of camphor in the absence of CDs.

The viscosity and conductivity of HPβCD/camphor-IC and HPγCD/camphor-IC solutions were measured at RT via Anton Paar Physica MCR 301 Rheometer equipped with a cone/plate accessory (spindle type CP 40-2) at a constant shear rate of 100 s<sup>-1</sup> and Inolab<sup>®</sup> pH/Cond 720-WTW, respectively.

Scanning electron microscopy (SEM, FEI-Quanta 200 FEG) was used to examine the morphology of electrospun HPβCD/camphor-IC-NF and HPγCD/camphor-IC-NF webs. Nanofibrous web samples were placed on metal stubs using double-sided copper tape and sputtered with 5 nm of Au/Pd (PECS-682) to minimize the charging during SEM imaging. AFD of the fibers was calculated directly from SEM images by measuring the diameter of about 100 fibers.

Five milliliters of water was added to camphor (powder), HPβCD/camphor-IC-NF, and HPγCD/camphor-IC-NF in petri dishes, and video (Supporting Video 1) was recorded for camphor and CD/camphor-IC-NF samples in order to show the water-solubility character of each sample.

20 mg/mL of each HPβCD/camphor-IC-NF and HPγCD/camphor-IC-NF was dissolved in d6-DMSO, and proton nuclear magnetic resonance (<sup>1</sup>H-NMR) spectra were recorded at 400 MHz (Bruker DPX-400). Then, the characteristic chemical shifts ( $\delta$ ) given in parts per million (ppm) corresponding to CD and camphor were determined, and the integrations were calculated via Mestrenova software. Finally, the molar ratio of CD and camphor in each CD/camphor-IC-NF was determined by the proportion of the peak belonging to CD and camphor.

Thermal properties of camphor, HPβCD-NF, HPβCD/camphor-IC-NF, HPγCD-NF, and HPγCD/camphor-IC-NF were investigated by thermogravimetric analysis (TGA, TA Q500) under nitrogen atmosphere by heating the nanofibrous webs starting from 25 °C at the heating rate of 20 °C/min.

Differential scanning calorimetry (DSC, TA Q2000) analyses were performed for camphor, HPβCD-NF, HPγCD-NF, HPβCD/camphor-IC-NF, and HPγCD/

camphor-IC-NF at a heating rate of 20 °C/min from 40 to 200 °C under nitrogen flow.

X-ray diffraction (XRD) (PANalytical X'Pert powder diffractometer) was used to examine the crystalline structure of camphor, HP $\beta$ CD-NF, HP $\gamma$ CD-NF, HP $\beta$ CD/camphor-IC-NF, and HP $\gamma$ CD/camphor-IC-NF at a range of  $2\theta = 5^\circ$ – $30^\circ$  using Cu K $\alpha$  radiation in powder diffraction configuration.

The infrared spectra of camphor, HP $\beta$ CD-NF, HP $\gamma$ CD-NF, HP $\beta$ CD/camphor-IC-NF, and HP $\gamma$ CD/camphor-IC-NF were recorded by Fourier transform infrared spectrometer (FTIR, Bruker-VERTEX 70). The samples were prepared as pellets by mixing them with potassium bromide (KBr) for the measurement. The scans (64 scans) were recorded between 4000 and 400  $\text{cm}^{-1}$  at the resolution of 4  $\text{cm}^{-1}$ .

The amount of camphor released from HP $\beta$ CD/camphor-IC-NF and HP $\gamma$ CD/camphor-IC-NF was measured using headspace gas chromatography–mass spectrometry (HS GC–MS) for 4 h at two different temperatures (37 and 75 °C). The Agilent Technologies 7890A gas chromatograph coupled with an Agilent Technologies 5975C inert MSD combined with a triple-axis detector was used. The capillary column was HP-5MS (Hewlett-Packard, Avondale, PA) (30 m  $\times$  0.25 mm i.d., 0.25  $\mu\text{m}$  film thickness). Ten milligrams of nanofibrous webs was put in a 20-mL headspace glass vial. The vials with the samples were agitated at 500 rpm. The syringe temperature was kept at 37 and 75 °C. Injection volume taken from the vials was 250  $\mu\text{L}$  of vapor to the HS GC–MS by using a headspace injector. The oven temperature was programmed as follows: initial 40 °C (held for 0.5 min at 40 °C), increased from 40 to 110 °C at a rate of 5 °C/min (held for 1 min at 110 °C). HS GC–MS was operated in a splitless and selected ion monitoring mode (SIM). NIST MS Search 2.0 library was used to identify the camphor peaks. The release experiments were performed in triplicate, and the results are reported as average  $\pm$  standard deviation.

### Computational method

We performed first-principles calculations based on density functional theory [26, 27] by using Vienna ab initio Simulation Package (VASP) [28, 29]. The exchange–correlation interaction is approximated by generalized gradient approximation (GGA-PBE) [30],

and the semiempirical dispersion potential is utilized to describe the van der Waals interactions [31]. The projector augmented-wave (PAW) potentials with kinetic energy cutoff 520 eV are used [32, 33]. This methodology is applied to optimize the positions of the atoms by setting convergence criteria on the total energy and force to  $10^{-4}$  eV and  $10^{-2}$  eV/ $\text{\AA}$ , respectively. The effect of solvent is modeled by considering implicit solvation model where continuum dielectric description is used [34].

## Results and discussion

### Phase solubility studies

Phase solubility diagrams of HP $\beta$ CD/camphor and HP $\gamma$ CD/camphor systems obtained in aqueous solution are shown in Fig. 2. The solubility of camphor increased linearly with the increasing amount of CD for both of the systems, and these diagrams are classified as  $A_L$  type. In addition, the linear improvement in the solubility of camphor confirms the presence of 1:1 complex [35, 36]. Such that, in the study of Tanaka et al. [37], it was observed that the solubility of camphor increased linearly as a function of concentration with HP $\beta$ CD and HP $\gamma$ CD. Therefore, it was concluded that the molar ratio of these complexes is 1:1 and the type of the diagram is  $A_L$ . In addition, the stability constant ( $K_C$ ) of HP $\beta$ CD/camphor-IC and HP $\gamma$ CD/camphor-IC calculated from the Eq. 1 was 229 and 251  $\text{M}^{-1}$ , respectively. As it is observed, HP $\gamma$ CD can form relatively more stable complexes with camphor molecules compared to HP $\beta$ CD.

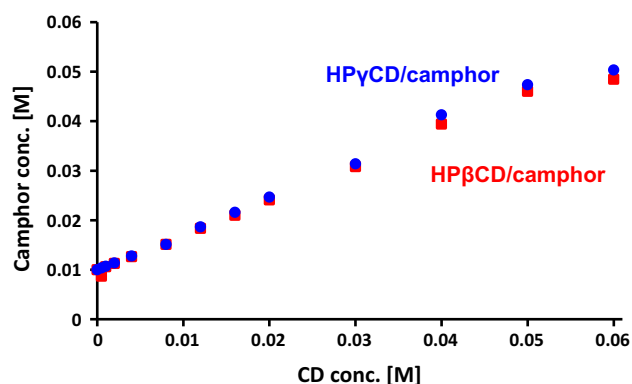


**Figure 2** Phase solubility diagram of HP $\beta$ CD/camphor and HP $\gamma$ CD/camphor systems in water ( $n = 3$ ).

In the earlier reports, different types of CDs were employed to obtain CD/camphor-ICs in powder form [37, 38]. In the study of Ciobanu et al. [38], stability constant and complexation efficiency of complexes formed between camphor and  $\alpha$ -CD,  $\beta$ -CD,  $\gamma$ -CD, hydroxypropyl- $\beta$ -cyclodextrin (HP $\beta$ CD), randomly methylated- $\beta$ -cyclodextrin (RAMEB), and of a low methylated- $\beta$ -cyclodextrin (CRYSMEB) and it was concluded that the stability constant was in the order of  $\beta$ -CD > CRYSMEB > HP $\beta$ CD > RAMEB >  $\gamma$ -CD >  $\alpha$ -CD. Tanaka et al. [37] produced inclusion complex of camphor with HP $\alpha$ CD, HP $\beta$ CD, and HP $\gamma$ CD. It was reported that HP $\beta$ CD significantly increased the solubility of camphor, and 1:1 stability constant of HP $\beta$ CD complexes was higher than that of other types of CDs. In addition, release rate of camphor was decreased by complexation with CDs, and rate of decrease was in agreement with the stability constant between CD and camphor. However, in case of our study, we have obtained relatively more stable complexation for HP $\gamma$ CD-based system compared to HP $\beta$ CD, and it will be discussed in the following sections.

### Computational modeling of CD/camphor-IC

In this study, the interaction of camphor molecule with HP $\beta$ CD and HP $\gamma$ CD was analyzed by using ab initio modeling techniques. Firstly, all the structures are relaxed in vacuum and then water without any constraint to obtain the optimized lowest energy configurations. Next, considering the center of mass of CD as origin, camphor molecule is approached to both of the CD through wider rim with different orientations. The four possible orientations of camphor and the variation of interaction energy are shown in Fig. 3a–d. The interaction energy ( $E_{\text{int}}$ ) for 1:1 stoichiometry is defined as:

$$E_{\text{int}} = E_{\text{T}}(\text{CD}) + E_{\text{T}}(\text{camphor}) - E_{\text{T}}(\text{IC}), \quad (2)$$

where  $E_{\text{T}}(\text{CD})$ ,  $E_{\text{T}}(\text{camphor})$ , and  $E_{\text{T}}(\text{IC})$  are the total energy of CD (HP $\beta$ CD or HP $\gamma$ CD), camphor, and their ICs (HP $\beta$ CD/camphor-IC and HP $\gamma$ CD/camphor-IC), respectively. Total energies are calculated both in vacuum and in solvent (water). Positive  $E_{\text{int}}$  indicates an attractive interaction between CD and camphor. The variation of  $E_{\text{int}}$  shows that there is no energy barrier for formation of IC indicating an exothermic reaction. For HP $\beta$ CD, camphor stays at wider rim and starts to deform HP tails when pushed

inside. For HP $\gamma$ CD, “dc” orientation of camphor where carbonyl group is close to the narrow rim is favored, whereas “ab” orientation is favored in case of HP $\beta$ CD. Kokkinout et al. [39] reported the results concerning computational modeling of enantiomers of camphor with  $\alpha$ -CD dimer, and one disordered camphor molecule is observed to occupy three major sites. Thus, carbonyl group of camphor pointing toward the primary rim of CD or carbonyl group is located on the CD dimer interface. We also obtain from our modeling results that “dc” orientation is one of the favorable orientations correlated with the literature.

According to the described computational model, IC is presumed to be formed when  $E_{\text{int}}$  is maximized which is at 3 and  $-1 \text{ \AA}$  for HP $\beta$ CD and HP $\gamma$ CD, respectively. The ground state configurations for HP $\beta$ CD/camphor and HP $\gamma$ CD/camphor are shown in Fig. 3. At this point,  $E_{\text{int}}$  is defined as the complexation energy ( $E_{\text{comp}}$ ) for 1:1 stoichiometry.  $E_{\text{comp}}$  is calculated as 22.78 and 23.63 kcal/mol for HP $\beta$ CD/camphor-IC and HP $\gamma$ CD/camphor-IC, respectively. Positive  $E_{\text{comp}}$  indicates that formation of IC is energetically favored between CD (HP $\beta$ CD and HP $\gamma$ CD) and camphor. We also checked the possibility of complex formation for 2:1 stoichiometry. While HP $\beta$ CD/camphor-IC is not formed in 2:1 stoichiometry due to size mismatch, HP $\gamma$ CD/camphor-IC is plausible. However,  $E_{\text{comp}}$  decreases for the second camphor molecule and becomes 11.02 kcal/mol. Therefore, it can be concluded from all these results that HP $\gamma$ CD tends to form slightly more stable complexes with camphor, compared to HP $\beta$ CD due to a more favorable allocation of camphor in HP $\gamma$ CD cavity.

The calculations are repeated in water for 1:1 stoichiometry to include the effect of solvent, and similar trends are obtained. However, upon interaction with water,  $E_{\text{comp}}$  decreases for both cases and becomes 16.54 and 16.99 kcal/mol for HP $\beta$ CD/camphor-IC and HP $\gamma$ CD/camphor-IC, respectively. The decrease in  $E_{\text{comp}}$  can be attributed to hydrophobic nature of CD cavity and camphor (because of the large hydrocarbon content). After revealing the interaction between CDs and camphor molecule, we analyzed the solubility of IC. The solubility of camphor in water is low ( $1.2 \text{ g dm}^{-3}$ ) but it can be enhanced by complex formation with CDs. However, the solubility cannot be estimated directly from our model, yet,

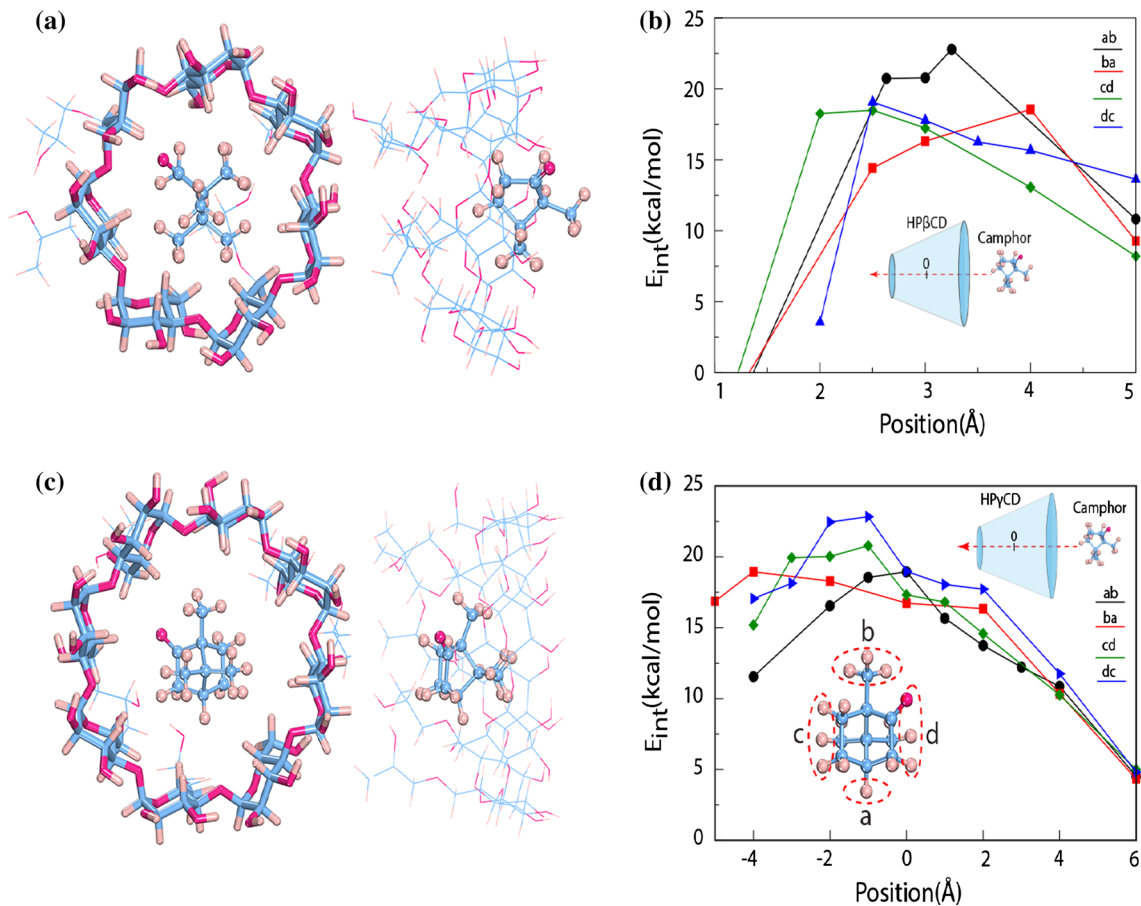


**Figure 3** **a** Top and side view of HPβCD/camphor-IC for 1:1 stoichiometry with “ab” orientation, **b** the variation of interaction energy of HPβCD and camphor with distance, **c** top and side view of HPγCD/camphor-IC for 1:1 stoichiometry with “dc”

solvation energy can be calculated which reveals the trend. Solvation energy ( $E_{\text{solv}}$ ) is defined as:

$$E_{\text{solv}} = E_{\text{T}}(\text{IC})_{\text{water}} - E_{\text{T}}(\text{IC})_{\text{vacuum}} \quad (3)$$

where  $E_{\text{T}}(\text{IC})_{\text{water}}$  and  $E_{\text{T}}(\text{IC})_{\text{vacuum}}$  are the total energy of HPβCD/camphor-IC and HPγCD/camphor-IC in water and vacuum, respectively.  $E_{\text{solv}}$  of camphor molecule is calculated as  $-3.79$  kcal/mol confirming the low solubility in water. On the other hand,  $E_{\text{solv}}$  is  $-70.71$  and  $-81.29$  kcal/mol for HPβCD/camphor-IC and HPγCD/camphor-IC, suggesting a substantial increase in solubility of the CD-IC system in water upon complexation.

### Morphology analysis of nanofibers

The representative SEM images of HPβCD/camphor-IC-NF and HPγCD/camphor-IC-NF are given in Fig. 1d–g. As confirmed from the SEM images, bead-

orientation, and **d** the variation of interaction energy of HPγCD and camphor with distance. The possible orientations of camphor are shown as inset. Blue, purple, and light pink balls represent carbon, oxygen, and hydrogen atoms, respectively.

free and uniform nanofibers were successfully electrospun from these CD/camphor-IC aqueous systems having such high concentrated solution (i.e., 160%, w/v). The use of such high concentration of CDs for the electrospinning of uniform nanofibers from pure CD [21, 22, 40, 41] systems and CD-IC [13–20] systems was optimized from our previous studies. It is worth mentioning that in this study, we have performed polymer-free electrospinning in which CD/camphor-IC aqueous systems are being electrospun without using a carrier polymeric matrix. Typically, high molecular weight polymers and high polymer concentrations are desirable for the electrospinning of nanofibers since polymer chain entanglements and overlapping are quite crucial for uniform fiber formation [42, 43]. For the electrospinning of small molecules such as CDs without using a carrier polymeric matrix, in our earlier studies

[13–22, 40, 41] we found out that highly concentrated solutions of CDs are required since self-aggregation of these supramolecular CD molecules helps the electrospinning of uniform fibers without the break of the jet.

Average fiber diameter (AFD) of HP $\beta$ CD/camphor-IC-NF and HP $\gamma$ CD/camphor-IC-NF was calculated as  $1330 \pm 440$  and  $1110 \pm 305$  nm, respectively. The slight difference in AFD of nanofibers could be due to the viscosity and conductivity differences between HP $\beta$ CD/camphor-IC and HP $\gamma$ CD/camphor-IC solutions (Table 1). In electrospinning, solutions having less viscosity and high conductivity yield thinner fibers due to the more stretching of the jet [43]. Here, both the viscosity and conductivity values of HP $\gamma$ CD/camphor-IC solution are lower than HP $\beta$ CD/camphor-IC solution (Table 1). It appears that HP $\gamma$ CD/camphor-IC-NF has slightly thinner AFD than HP $\beta$ CD/camphor-IC-NF possibly due to the low viscosity of the HP $\gamma$ CD/camphor-IC solution. After electrospinning of CD/camphor-IC systems, self-standing and flexible nanofibrous webs of HP $\beta$ CD/camphor-IC-NF and HP $\gamma$ CD/camphor-IC-NF were obtained as depicted in Fig. 1f, g. Even though the electrospun nanofibers are made of non-polymeric CD/camphor-IC systems, both HP $\beta$ CD/camphor-IC-NF and HP $\gamma$ CD/camphor-IC-NF nanofibrous webs have shown flexible character (Fig. 1f, g). Moreover, we have shown that these CD/camphor-IC-NF nanofibrous webs are readily soluble in water. Here, solubility tests were done by pouring 5 mL of water on camphor, HP $\beta$ CD/camphor-IC-NF, and HP $\gamma$ CD/camphor-IC-NF (Supporting Video 1). Camphor could not be dissolved in water, and on the other hand, the CD/camphor-IC-NF nanofibrous webs were dissolved within 2 s and CD makes the camphor soluble in water, as also confirmed by the phase solubility tests (Fig. 2).

### The molar ratio of CD/camphor-IC

The presence and the molar ratio of camphor in the electrospun CD/camphor-IC-NF samples were confirmed by proton nuclear magnetic resonance ( $^1\text{H-NMR}$ ). The  $^1\text{H-NMR}$  spectra of HP $\beta$ CD/camphor-IC-NF and HP $\gamma$ CD/camphor-IC-NF dissolved in  $d_6$ -DMSO are presented in Fig. 4a, b. The initial molar ratio of HP $\beta$ CD:camphor and HP $\gamma$ CD:camphor was prepared as 1:1 prior to electrospinning of CD/camphor-IC aqueous solutions. After electrospinning, the

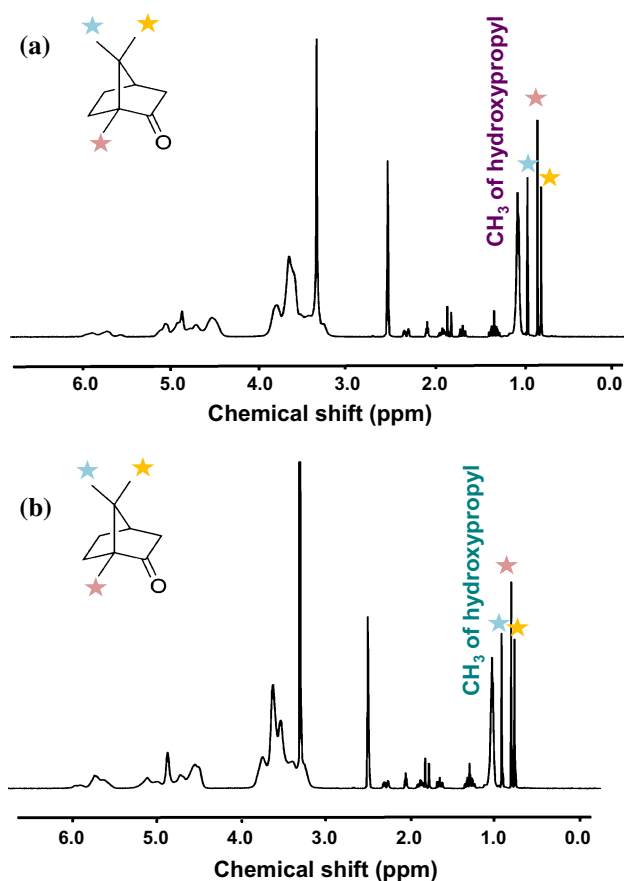


**Figure 4**  $^1\text{H-NMR}$  spectra of **a** HP $\beta$ CD/camphor-IC-NF and **b** HP $\gamma$ CD/camphor-IC-NF dissolved in  $d_6$ -DMSO.

molar ratio of HP $\beta$ CD:camphor and HP $\gamma$ CD:camphor in HP $\beta$ CD/camphor-IC-NF and HP $\gamma$ CD/camphor-IC-NF was determined as  $\sim 1.00:0.65$  and  $\sim 1.00:0.90$ , respectively. For molar ratio calculation from  $^1\text{H-NMR}$  spectrum, the proportion of the peaks belonging to CD and camphor at 1 and 0.9 ppm, respectively, were taken into account. The  $^1\text{H-NMR}$  studies revealed that  $\sim 65$  and  $\sim 90\%$  of the initial amount of camphor were preserved in HP $\beta$ CD/camphor-IC-NF and HP $\gamma$ CD/camphor-IC-NF, respectively. Although camphor is a volatile compound, substantial amount of camphor was preserved after electrospinning in the CD/camphor-IC-NF samples owing to the inclusion complexation between camphor and CD (HP $\beta$ CD and HP $\gamma$ CD) in the fiber matrix. It was also noticed that HP $\gamma$ CD/camphor-IC-NF has preserved higher amount of camphor when compared to HP $\beta$ CD/camphor-IC-NF. This is probably originated from the higher complexation efficiency of HP $\gamma$ CD with camphor due to wider cavity of HP $\gamma$ CD which

provides a better localization and specific interaction for camphor when compared to HP $\beta$ CD, which was also indicated by the modeling and phase solubility results.

### Thermal analysis of nanofibers

Camphor has a volatile nature; therefore, it is of importance for camphor molecules to be protected from evaporation. Here, thermal stability of camphor in HP $\beta$ CD/camphor-IC-NF and HP $\gamma$ CD/camphor-IC-NF samples was investigated by TGA (Fig. 5). Thermal evaporation of pure camphor starts at around 40 °C and completely evaporated below 150 °C. In order to better analyze the TGA data of CD/camphor-IC-NF samples, the thermal behavior of electrospun pure CD nanofibers (HP $\beta$ CD-NF and

HP $\gamma$ CD-NF) was also examined for comparison. Both pure HP $\beta$ CD-NF and HP $\gamma$ CD-NF exhibited two steps of weight loss below 100 °C and between 275 and 400 °C corresponding to water loss and main thermal degradation of CD, respectively. The water in HP $\beta$ CD-NF and HP $\gamma$ CD-NF was also calculated as  $\sim 4.80$  and  $\sim 5.75\%$  from the water loss of each CD type. The TGA data reveal that thermal stability of camphor was improved by inclusion complexation for both HP $\beta$ CD/camphor-IC-NF and HP $\gamma$ CD/camphor-IC-NF (Fig. 5a, b). Four stages of weight loss observed for HP $\beta$ CD/camphor-IC-NF: below 100, 180–250, 250–300, and 300–415 °C, which was attributed to the water loss, evaporation of camphor in two steps, and main degradation of HP $\beta$ CD, respectively. For HP $\gamma$ CD/camphor-IC-NF sample, the first weight loss below 100 °C was related to the water loss, the second weight loss at around 195–260 °C is due to the thermal evaporation of camphor, and the third weight loss between 325 and 400 °C is the thermal degradation of HP $\gamma$ CD. In brief, when compared to pure camphor, the thermal evaporation of camphor has shifted to much higher temperature (above 200 °C) in CD/camphor-IC-NF samples, which is due to the inclusion complexation between camphor and CD in the nanofiber matrix. So, the thermal stability enhancement of camphor has been successfully achieved by encapsulation of camphor in electrospun polymer-free CD-IC nanofiber matrix. In addition, the amount of water in HP $\beta$ CD/camphor-IC-NF and HP $\gamma$ CD/camphor-IC-NF was calculated to be  $\sim 1.15$  and  $\sim 1.50\%$ , which are lower than the amount of water present in HP $\beta$ CD-NF and HP $\gamma$ CD-NF. Since the water in the cavity of HP $\beta$ CD and HP $\gamma$ CD was replaced with camphor during complex formation. This result is another support for complexation of camphor with HP $\beta$ CD and HP $\gamma$ CD.

Figure 6a represents DSC thermograms of camphor, HP $\beta$ CD-NF, HP $\gamma$ CD-NF, HP $\beta$ CD/camphor-IC-NF, and HP $\gamma$ CD/camphor-IC-NF. Camphor exhibited an endothermic peak at around 175 °C that corresponds to its melting point, whereas the melting point of camphor was not observed in HP $\beta$ CD/camphor-IC-NF and HP $\gamma$ CD/camphor-IC-NF. The disappearance of thermal transitions such as melting point [12, 44] or glass transition [19] of guest molecules in the presence of CDs is well known, which is used to confirm the formation of inclusion complexes between CDs and guest molecules. Hence, the absence of melting point of camphor in

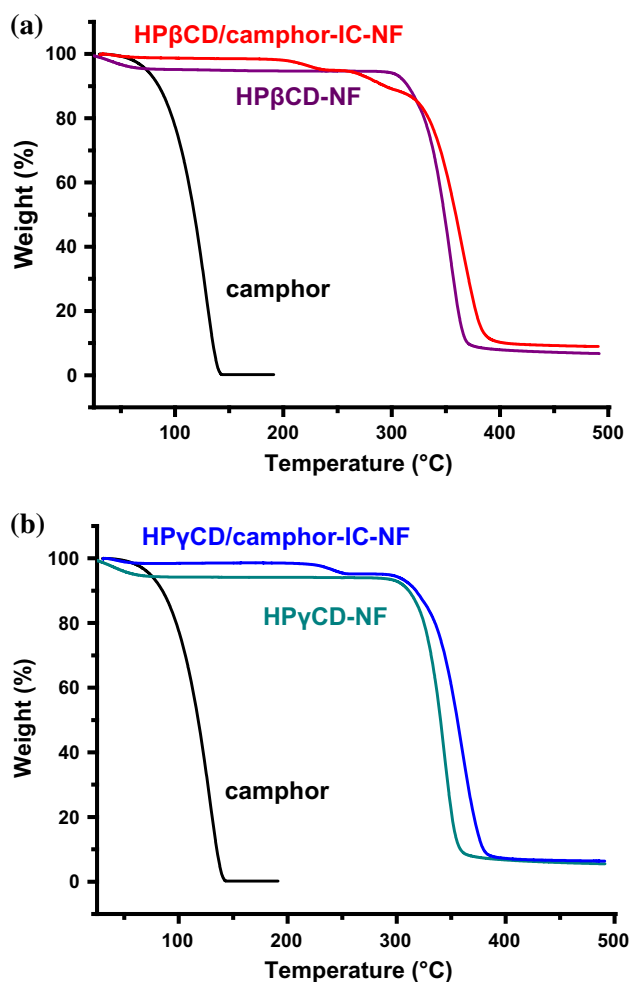


**Figure 5** TGA thermograms of **a** camphor, HP $\beta$ CD-NF, HP $\beta$ CD/camphor-IC-NF and **b** camphor, HP $\gamma$ CD-NF, HP $\gamma$ CD/camphor-IC-NF.

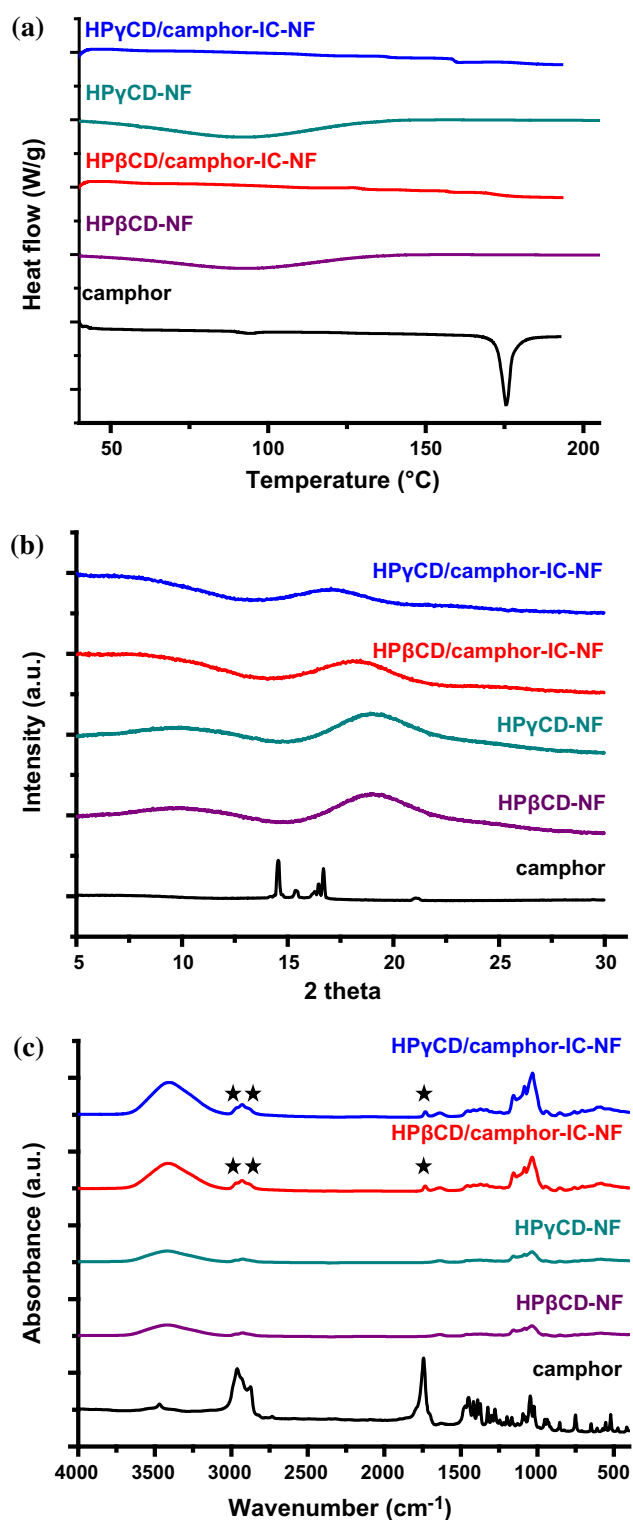


**Figure 6** **a** DSC thermograms of camphor, HPβCD-NF, HPβCD/camphor-IC-NF, HPγCD-NF, and HPγCD/camphor-IC-NF; **b** XRD patterns of camphor, HPβCD-NF, HPγCD-NF, HPβCD/camphor-IC-NF, and HPγCD/camphor-IC-NF, **c** FTIR spectra of camphor, HPβCD-NF, HPγCD-NF, HPβCD/camphor-IC-NF, and HPγCD/camphor-IC-NF.

CD/camphor-IC-NFs further confirms the inclusion complexation state of camphor within CD cavity in this nanofiber matrix. The dehydration of CDs in HPβCD-NF and HPγCD-NF is observed as typical broad endothermic peaks between 25 and 160 and 25–155 °C, respectively. However, HPβCD/camphor-IC-NF and HPγCD/camphor-IC-NF did not exhibit any dehydration peak, which is a support for camphor to be included in the cavity of CDs by replacing the water in the cavity. HPβCD/camphor-IC-NF and HPγCD/camphor-IC-NF have only low amount of water as confirmed by TGA results.

### Structural characterization of nanofibers

The XRD studies were performed for camphor, HPβCD-NF, HPγCD-NF, HPβCD/camphor-IC-NF, and HPγCD/camphor-IC-NF, and the resulting diffraction patterns are displayed in Fig. 6b. Camphor is a crystalline molecule with sharp diffraction peaks at 14.5°, 15.4°, 16.5°, and 16.7°, whereas HPβCD-NF and HPγCD-NF exhibited amorphous pattern. Characteristic crystalline peaks of camphor disappeared in the diffraction pattern of HPβCD/camphor-IC-NF and HPγCD/camphor-IC-NF. This result is the proof inclusion complexation between camphor and CD, suggesting that camphor molecules are included inside the CD cavity and they are separated from each other by CD molecules where camphor molecules cannot form crystals. Hence, the absence of a camphor diffraction peak in CD/camphor-IC-NF samples strongly suggests that camphor is encapsulated as an inclusion complex within the CD nanofiber matrix after electrospinning.

FTIR analyses were also performed for camphor, HPβCD-NF, HPγCD-NF, HPβCD/camphor-IC-NF, and HPγCD/camphor-IC-NF (Fig. 6c). The characteristic absorption peaks of pure CDs were observed at around 1030, 1080, and 1157  $\text{cm}^{-1}$  due to the coupled C–C and C–O stretching vibrations and antisymmetric stretching vibration of the C–O–C glycosidic bridge; 1638, 2925, and 3401  $\text{cm}^{-1}$  corresponding to H–OH bending, C–H stretching, and O–H stretching, respectively [15, 17]. The characteristic absorption peaks of camphor are observed at around 3466, 2961, 2870, 1739, 1624, 1476, 1445, 1387, 1245, 1153, 1126, and 1095  $\text{cm}^{-1}$  [45]. Most of the camphor peaks overlap in the 1500–1000  $\text{cm}^{-1}$  range with the characteristic peaks of CDs, which makes it difficult to analyze the FTIR spectra of HPβCD/camphor-IC-

NF and HP $\gamma$ CD/camphor-IC-NF in this range. Nonetheless, the camphor peaks at around 2960 and 2871  $\text{cm}^{-1}$  also exist in the FTIR spectra of HP $\beta$ CD/camphor-IC-NF and HP $\gamma$ CD/camphor-IC-NF. However, due to the interaction between camphor and CDs, camphor peaks shifted to 2964 and 2879  $\text{cm}^{-1}$  for HP $\beta$ CD/camphor-IC-NF and 2963 and 2875  $\text{cm}^{-1}$  for HP $\gamma$ CD/camphor-IC-NF. But, the higher intensity of the camphor peaks (2960 and 2871  $\text{cm}^{-1}$ ) in the spectra of HP $\beta$ CD/camphor-IC-NF and HP $\gamma$ CD/camphor-IC-NF as compared to pure CD-NF samples confirms the presence of camphor in these CD/camphor-IC-NF samples. In addition, the salient peak of camphor at 1740  $\text{cm}^{-1}$  is obviously seen in the FTIR spectra of HP $\beta$ CD/camphor-IC-NF and HP $\gamma$ CD/camphor-IC-NF at 1742  $\text{cm}^{-1}$ , and this further confirms the existence of camphor in the CD/camphor-IC-NF samples. In addition, shifting of this peak from 1740 to 1742  $\text{cm}^{-1}$  shows the presence of an interaction between camphor and CDs, which further suggests the inclusion complex formation.

### Release study

The release of camphor from HP $\beta$ CD/camphor-IC-NF and HP $\gamma$ CD/camphor-IC-NF was measured at 37 and 75  $^{\circ}\text{C}$ , and the results are given in Fig. 7. The release of camphor increased as the temperature

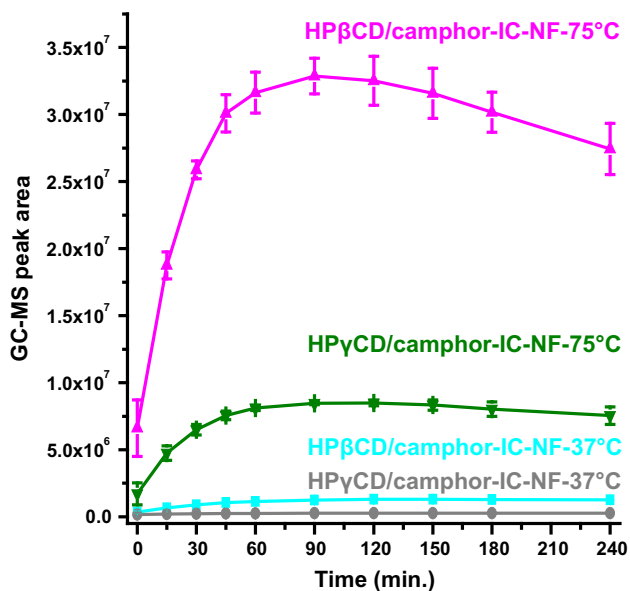


**Figure 7** Cumulative release of camphor from HP $\beta$ CD/camphor-IC-NF and HP $\gamma$ CD/camphor-IC-NF at 37 and 75  $^{\circ}\text{C}$  ( $n = 3$ ). The error bars in the figure represent the standard deviation.

increased from 37 and 75  $^{\circ}\text{C}$  in both HP $\beta$ CD/camphor-IC-NF and HP $\gamma$ CD/camphor-IC-NF owing to the diffusion coefficient increment of the camphor molecules [46]. The preserved amount of camphor is calculated less from  $^1\text{H-NMR}$  in HP $\beta$ CD/camphor-IC-NF, but the total released amount of camphor is much more both at 37 and 75  $^{\circ}\text{C}$  as compared to HP $\gamma$ CD/camphor-IC-NF. Despite its lower encapsulation efficiency, the reason for the higher release amount of HP $\beta$ CD/camphor-IC-NF compared to HP $\gamma$ CD/camphor-IC-NF might be originated from the slightly weaker interaction of HP $\beta$ CD and camphor, which was revealed by the phase solubility and modeling studies. Moreover, when we consider the favorable allocation of camphor molecules inside the CD cavity demonstrated by the modeling study, camphor prefers to position at the edge of the wider rim of CD molecules in case of HP $\beta$ CD (Fig. 3a), which most probably leads to easier release of guest molecules from the cavity of HP $\beta$ CD compared to HP $\gamma$ CD. On the contrary, camphor molecules prefer to locate at inner side of the narrow rim of HP $\gamma$ CD, which might create a more stable interaction for camphor by the steric hindrance of hydroxypropyl moieties. The calculated higher encapsulation efficiency of HP $\gamma$ CD/camphor-IC-NF ( $\sim 1.00:0.90$ ) than HP $\beta$ CD/camphor-IC-NF ( $\sim 1.00:0.65$ ) might be also based on this positioning differences of these two CD types, such that weaker interaction of HP $\beta$ CD/camphor-IC might allow easier evaporation of camphor during electrospinning and storage.

### Conclusion

Inclusion complexes (ICs) from two kinds of CD derivatives (HP $\beta$ CD and HP $\gamma$ CD) and camphor which is known for its volatile and hydrophobic nature were formed in highly concentrated aqueous solutions for the electrospinning of nanofibers (HP $\beta$ CD/camphor-IC-NF and HP $\gamma$ CD/camphor-IC-NF). The phase solubility studies indicated the water-solubility increase of camphor with CD, and the 1:1 molar ratio was observed for these inclusion complexes (HP $\beta$ CD/camphor-IC and HP $\gamma$ CD/camphor-IC). In addition, the stability constant calculated for HP $\gamma$ CD/camphor-IC was higher than HP $\beta$ CD/camphor-IC, suggesting that HP $\gamma$ CD can form relatively more stable inclusion complexes with camphor when compared to HP $\beta$ CD. Computational modeling

studies also showed that the interaction between camphor and HP $\gamma$ CD is slightly stronger than the interaction with HP $\beta$ CD due to the better allocation of camphor in HP $\gamma$ CD, which leads to more favorable interaction compare to HP $\beta$ CD. In addition, computational modeling study also indicated that the preferential orientation of camphor is variable depending on the CD types. After electrospinning of these CD/camphor-IC solutions without using any polymer template, self-standing and flexible nanofibrous webs of HP $\beta$ CD/camphor-IC-NF and HP $\gamma$ CD/camphor-IC-NF were produced. These CD/camphor-IC-NF webs have shown fast-dissolving characteristic, and camphor was become readily water soluble. Even camphor is quite a volatile molecule, the initial molar ratio of CD:camphor (1:1) in CD/camphor-IC solutions was significantly preserved after electrospinning of CD/camphor-IC-NF samples. The CD:camphor molar ratio was determined from  $^1\text{H-NMR}$  studies, and it was found to be  $\sim 1.00:0.65$  and  $\sim 1.00:0.90$  for HP $\beta$ CD/camphor-IC-NF and HP $\gamma$ CD/camphor-IC-NF, respectively. The DSC, XRD, and FTIR studies confirmed that the inclusion complexation state was present between CD and camphor after electrospinning of HP $\beta$ CD/camphor-IC-NF and HP $\gamma$ CD/camphor-IC-NF nanofibrous webs. TGA studies revealed the improvement in the thermal stability of camphor when it is included in the cavity of CDs in CD/camphor-IC-NFs. The release of camphor from CD/camphor-IC-NFs was measured at 37 and 75 °C, and less amount of camphor was released from HP $\gamma$ CD/camphor-IC-NF possibly due to the stronger interaction between HP $\gamma$ CD and camphor as suggested by the phase solubility results and computational modeling studies.

## Acknowledgements

Dr. A. Celebioglu thanks TUBITAK-BIDEB for the Ph.D. scholarship. Dr. Z. Aytac thanks TUBITAK-BIDEB and TUBITAK (Project # 213M185) for the Ph.D. scholarship.

**Funding** Dr. Uyar acknowledges the Scientific and Technological Research Council of Turkey (TUBITAK)—Turkey (Project # 213M185) for funding this research. Dr. Uyar and Dr. Durgun also acknowledge the partial support from the Turkish Academy of

Sciences—Outstanding Young Scientists Award Program (TUBA-GEBIP)—Turkey. The computational resources are provided by TUBITAK ULAKBIM, High Performance and Grid Computing Center (TR-Grid e-Infrastructure), and the National Center for High Performance Computing of Turkey (UHem) under Grant No. 5003622015.

**Electronic supplementary material:** The online version of this article (<https://doi.org/10.1007/s10853-017-1918-4>) contains supplementary material, which is available to authorized users.

## References

- [1] Bakkali F, Averbeck S, Averbeck D, Idaomar M (2008) Biological effects of essential oils—a review. *Food Chem Toxicol* 46(2):446–475
- [2] El Asbahani A, Miladi K, Badri W, Sala M, Addi EA, Casabianca H, El Mousadik A, Hartmann D, Jilale DA, Renaud FNR, Elaissari A (2015) Essential oils: from extraction to encapsulation. *Int J Pharm* 483(1):220–243
- [3] Uyar T, Kny E (eds) (2017) *Electrospun materials for tissue engineering and biomedical applications: research, design and commercialization*. Woodhead Publishing, Cambridge
- [4] Wen P, Wen Y, Zong M-H, Linhardt RJ, Wu H (2017) Encapsulation of bioactive compound in electrospun fibers and its potential application. *J Agric Food Chem* 65:9161–9179
- [5] Wendorff JH, Agarwal S, Greiner A (2012) *Electrospinning: materials, processing, and applications*. Wiley, Weinheim
- [6] Bilensoy E (ed) (2011) *Cyclodextrins in pharmaceuticals, cosmetics, and biomedicine: current and future industrial applications*. Wiley, Hoboken, New Jersey
- [7] Del Valle EM (2004) Cyclodextrins and their uses: a review. *Process Biochem* 39(9):1033–1046
- [8] Szejtli J (1998) Introduction and general overview of cyclodextrin chemistry. *Chem Rev* 98(5):1743–1754
- [9] Aytac Z, Dogan SY, Tekinay T, Uyar T (2014) Release and antibacterial activity of allyl isothiocyanate/ $\beta$ -cyclodextrin complex encapsulated in electrospun nanofibers. *Colloids Surf B* 120:125–131
- [10] Aytac Z, Ipek S, Durgun E, Tekinay T, Uyar T (2017) Antibacterial electrospun zein nanofibrous web encapsulating thymol/cyclodextrin-inclusion complex for food packaging. *Food Chem* 233:117–124
- [11] Uyar T, Hacıoğlu J, Besenbacher F (2009) Electrospun polystyrene fibers containing high temperature stable volatile

- fragrance/ flavor facilitated by cyclodextrin inclusion complexes. *React Funct Polym* 69(3):145–150
- [12] Kayaci F, Uyar T (2012) Encapsulation of vanillin/cyclodextrin inclusion complex in electrospun polyvinyl alcohol (PVA) nanowebs: prolonged shelf-life and high temperature stability of vanillin. *Food Chem* 133(3):641–649
- [13] Celebioglu A, Uyar T (2011) Electrospinning of polymer-free nanofibers from cyclodextrin inclusion complexes. *Langmuir* 27(10):6219–6226
- [14] Celebioglu A, Umu OC, Tekinay T, Uyar T (2014) Antibacterial electrospun nanofibers from triclosan/cyclodextrin inclusion complexes. *Colloids Surf B* 116:612–619
- [15] Aytac Z, Yildiz ZI, Kayaci-Senirmak F, San Keskin NO, Tekinay T, Uyar T (2016) Electrospinning of polymer-free cyclodextrin/geraniol-inclusion complex nanofibers: enhanced shelf-life of geraniol with antibacterial and antioxidant properties. *RSC Adv* 6(52):46089–46099
- [16] Celebioglu A, Kayaci-Senirmak F, Ipek S, Durgun E, Uyar T (2016) Polymer-free nanofibers from vanillin/cyclodextrin inclusion complexes: high thermal stability, enhanced solubility and antioxidant property. *Food Funct* 7(7):3141–3153
- [17] Aytac Z, Yildiz ZI, Kayaci-Senirmak F, San Keskin NO, Kusku SI, Durgun E, Tekinay T, Uyar T (2016) Fast-dissolving, prolonged release, and antibacterial cyclodextrin/limonene-inclusion complex nanofibrous webs via polymer-free electrospinning. *J Agric Food Chem* 64(39):7325–7334
- [18] Aytac Z, Yildiz ZI, Kayaci-Senirmak F, Tekinay T, Uyar T (2017) Electrospinning of cyclodextrin/linalool-inclusion complex nanofibers: fast-dissolving nanofibrous web with prolonged release and antibacterial activity. *Food Chem* 231:192–201
- [19] Celebioglu A, Uyar T (2017) Antioxidant vitamin E/cyclodextrin inclusion complex electrospun nanofibers: enhanced water-solubility, prolonged shelf-life and photostability of vitamin E. *J Agric Food Chem* 65(26):5404–5412
- [20] Celebioglu A, Yildiz ZI, Uyar T (2017) Electrospun nanofibers from cyclodextrin inclusion complexes with cineole and p-cymene: enhanced water solubility and thermal stability. *Int J Food Sci Technol*. <https://doi.org/10.1111/ijfs.13564>
- [21] Celebioglu A, Uyar T (2010) Cyclodextrin nanofibers by electrospinning. *Chem Commun* 46(37):6903–6905
- [22] Celebioglu A, Uyar T (2012) Electrospinning of nanofibers from non-polymeric systems: polymer-free nanofibers from cyclodextrin derivatives. *Nanoscale* 4(2):621–631
- [23] Chang CP, Leung TK, Lin SM, Hsu CC (2006) Release properties on gelatin-gum arabic microcapsules containing camphor oil with added polystyrene. *Colloids Surf B* 50(2):136–140
- [24] Higuchi TK, Connors A (1965) Phase-solubility techniques. *Adv Anal Chem Instrum* 4:117–212
- [25] Yalkowsky SH, He Y, Jain P (2016) Handbook of aqueous solubility data. CRC Press, Boca Raton
- [26] Kohn W, Sham LJ (1965) Self-consistent equations including exchange and correlation effects. *Phys Rev* 140(4A):A1133–A1138
- [27] Hohenberg P, Kohn W (1964) Inhomogeneous electron gas. *Phys Rev* 136(3B):B864–B871
- [28] Kresse G, Furthmüller J (1996) Efficient iterative schemes for ab initio total-energy calculations using a plane-wave basis set. *Phys Rev B* 54(16):11169–11186
- [29] Kresse G, Furthmüller J (1996) Efficiency of ab initio total energy calculations for metals and semiconductors using a plane-wave basis set. *Comput Mater Sci* 6(1):15–50
- [30] Perdew JP, Burke K, Ernzerhof M (1996) Generalized gradient approximation made simple. *Phys Rev Lett* 77(18):3865–3868
- [31] Grimme S (2006) Semiempirical GGA-type density functional constructed with a long-range dispersion correction. *J Comput Chem* 27(15):1787–1799
- [32] Blöchl PE (1994) Projector augmented-wave method. *Phys Rev B* 50(24):17953–17979
- [33] Kresse G, Joubert D (1999) From ultrasoft pseudopotentials to the projector augmented-wave method. *Phys Rev B* 59(3):1758–1775
- [34] Mathew K, Sundararaman R, Letchworth-Weaver K, Arias TA, Hennig RG (2014) Implicit solvation model for density-functional study of nanocrystal surfaces and reaction pathways. *J Chem Phys* 140(8):084106–084108
- [35] Aleem O, Kuchekar B, Pore Y, Late S (2008) Effect of  $\beta$ -cyclodextrin and hydroxypropyl  $\beta$ -cyclodextrin complexation on physicochemical properties and antimicrobial activity of cefdinir. *J Pharm Biomed Anal* 47(3):535–540
- [36] Pralhad T, Rajendrakumar K (2004) Study of freeze-dried quercetin-cyclodextrin binary systems by DSC, FT-IR, X-ray diffraction and SEM analysis. *J Pharm Biomed Anal* 34(2):333–339
- [37] Tanaka M, Matsuda H, Sumiyoshi H, Arima H, Hirayama F, Uekama K, Tsuchiya S (1996) 2-Hydroxypropylated cyclodextrins as a sustained-release carrier for fragrance materials. *Chem Pharm Bull* 44(2):416–420
- [38] Ciobanu A, Landy D, Fourmentin S (2013) Complexation efficiency of cyclodextrins for volatile flavor compounds. *Food Res Int* 53(1):110–114
- [39] Kokkinou A, Tsorteki F, Karpusas M, Papakyriakou A, Bethanis K, Mentzafos D (2010) Study of the inclusion of the (R)- and (S)-camphor enantiomers in  $\alpha$ -cyclodextrin by

- X-ray crystallography and molecular dynamics. *Carbohydr Res* 345(8):1034–1040
- [40] Celebioglu A, Uyar T (2013) Electrospun gamma-cyclodextrin ( $\gamma$ -CD) nanofibers for the entrapment of volatile organic compounds. *RSC Adv* 3(45):22891–22895
- [41] Celebioglu A, Uyar T (2013) Electrospinning of nanofibers from non-polymeric systems: electrospun nanofibers from native cyclodextrins. *J Colloid Interface Sci* 404:1–7
- [42] Shenoy SL, Bates WD, Frisch HL, Wnek GE (2005) Role of chain entanglements on fiber formation during electrospinning of polymer solutions: good solvent, non-specific polymer-polymer interaction limit. *Polymer* 46(10):3372–3384
- [43] Uyar T, Besenbacher F (2008) Electrospinning of uniform polystyrene fibers: the effect of solvent conductivity. *Polymer* 49(24):5336–5343
- [44] Aytac Z, Sen HS, Durgun E, Uyar T (2015) Sulfoxazole/cyclodextrin inclusion complex incorporated in electrospun hydroxypropyl cellulose nanofibers as drug delivery system. *Colloids Surf B* 128:331–338
- [45] Wang C, Wang H, Liu Y (2016) Purification of Pb(II) ions from aqueous solution by camphor leaf modified with succinic anhydride. *Colloids Surf A* 509:80–85
- [46] Hu CY, Chen M, Wang ZW (2012) Release of thymol, cinnamaldehyde and vanillin from soy protein isolate films into olive oil. *Packag Technol Sci* 25(2):97–106